Microfabricated Silicon Solid Immersion Lens

Daniel A. Fletcher, Kenneth B. Crozier, Kathryn W. Guarini, *Member, IEEE*, Stephen C. Minne, Gordon S. Kino, *Life Fellow, IEEE*, Calvin F. Quate, *Life Fellow, IEEE*, and Kenneth E. Goodson, *Associate Member, IEEE*

***Abstract*—We present the microfabrication of a solid immersion lens from silicon for scanning near-field optical microscopy. The solid immersion lens (SIL) achieves spatial resolution better than the diffraction limit in air without the losses associated with tapered optical fibers. A 15-μm-diameter SIL is formed by reflowing photoresist in acetone vapor and transferring the shape into single-crystal Si with reactive ion etching. The lens is integrated onto a cantilever for scanning, and a tip is fabricated opposite the lens to localize lens-sample contact. Using the Si SIL, we show that microfabricated lenses have greater optical transparency and less aberration than conventional lenses by focusing a plane wave of 633-nm light to a spot close to a wavelength in diameter. Microlenses made from absorbing materials can be used when the lens thickness is comparable to the penetration depth of the light. Tolerance to errors in curvature and thickness is improved in micromachined lenses, because spherical aberrations decrease with lens diameter. We demonstrate scanning near-field optical microscopy with the Si SIL and achieve spatial resolution below the diffraction limit in air by resolving 200-nm lines with 633-nm light. [648]**

***Index Terms*—Atomic force microscopy, microelectromechanical devices, micromatching, microscopy, optical imaging.**

I. Introduction

SCANNING probes used for scanning tunneling microscopy (STM) and atomic force microscopy (AFM) characterize surfaces through local electric, magnetic, or mechanical interactions. Optical imaging below the diffraction limit is performed by scanning a subwavelength source such as a tapered optical fiber above the surface, a technique known as scanning near-field optical microscopy (SNOM) [1]. This approach suffers from low optical throughput and difficulty manufacturing reliable apertures. An alternate and more efficient technique for high-resolution optical imaging is solid immersion microscopy. This technique uses a lens held close to a sample to improve spatial resolution by a factor proportional to the refractive index of the lens [2].

The spatial resolution of a lens without aberration is limited by diffraction of light from the lens aperture. The minimum full-width at half-maximum (FWHM) spot size s is $\lambda/(2NA)$ in the scalar approximation, where λ is the free space wavelength, $NA = n\sin\theta$ is the numerical aperture, θ is the maximum angle of rays in the focused beam, and n is the index of refraction at the focus. The spot size of focused light s also corresponds to the Sparrow criteria for two-point spatial resolution of the system [3]. Fig. 1(a) shows light focused on a sample in air with a maximum angle θ and through a hemispherical solid immersion lens (SIL) of index n and radius a with the same maximum angle θ. When light is focused onto the flat surface at the geometrical center of the lens, the effective wavelength inside the SIL is reduced by a factor $1/n$, and the spot size is reduced by the same factor from its value in air. The focused spot sizes of the two cases are calculated with the vector diffraction theory of Richards and Wolf [4] and given in Fig. 1(b). In a superspherical SIL, light is focused to a point a/n below the geometrical center, and refraction at the lens surface increases the maximum angle of the light within the lens. Like the hemispherical SIL, the NA of the superspherical SIL can be increased to a maximum value of n:

We report the microfabrication of a 15-μm-diameter solid immersion lens from single-crystal silicon for scanning near-field optical microscopy. Spatial resolution is governed by the size of the focused spot in Si ($n = 3.4$ at $\lambda = 1.0$ μm) rather than in air. The microlens has the advantage that it is thin enough to transmit light at wavelengths where Si is absorbing. In addition, the microlens has less spherical aberration than larger diameter lenses, so lens shape is less critical than it is for conventional SILs. We demonstrate focusing with the microfabricated Si SIL at $\lambda = 633$ nm and use the scanning SIL to resolve 200-nm lines in transmission mode.

II. Solid Immersion Microscopy

Conventional solid immersion lenses are made by lapping and grinding techniques and have diameters of 1 mm or larger. They have been used to improve spatial resolution in a variety of applications. However, the problem of maintaining a sufficiently small spacing between the SIL and sample limits the use of conventional SIL's and motivates the microfabrication of SILs on cantilevers for scanning near-field optical microscopy.

A. Applications of Solid Immersion Microscopy

Recent applications of solid immersion microscopy have included imaging, data storage, and photolithography. Mansfield and Kino imaged 100-nm lines using 436-nm light and a hemispherical SIL, reaching $NA = 1.5$ [2]. Sasaki *et al.*studied photoluminescence of quantum wells at low-temperatures using a superspherical TaF-3 glass SIL [5], and Wu *et al.* demonstrated $NA = 2.0$ using a hemispherical GaP SIL [6]. Ghislain and Elings scanned a superspherical cubic zirconia SIL with $NA = 1.5$ [7].

Manuscript received November 21, 2000. This work was supported by the Department of Energy, Semiconductor Research Corporation, Office of Naval Research, and the National Science Foundation. The authors made use of the Stanford Nanofabrication Facility, part of the National Nanofabrication Users Network funded by the NSF. Subject Editor O. Tabata.

D. A. Fletcher, K. B. Crozier, S. C. Minne, G. S. Kino, C. F. Quate, and K. E. Goodson are with the E. L. Ginzton Laboratory, Stanford University, Stanford, CA 94305 USA (e-mail: dan.fletcher@stanford.edu).

K. W. Guarini is with IBM T. J. Watson Research Center, Yorktown Heights, NY 10598 USA.

Publisher Item Identifier S 1057-7157(01)05029-6.

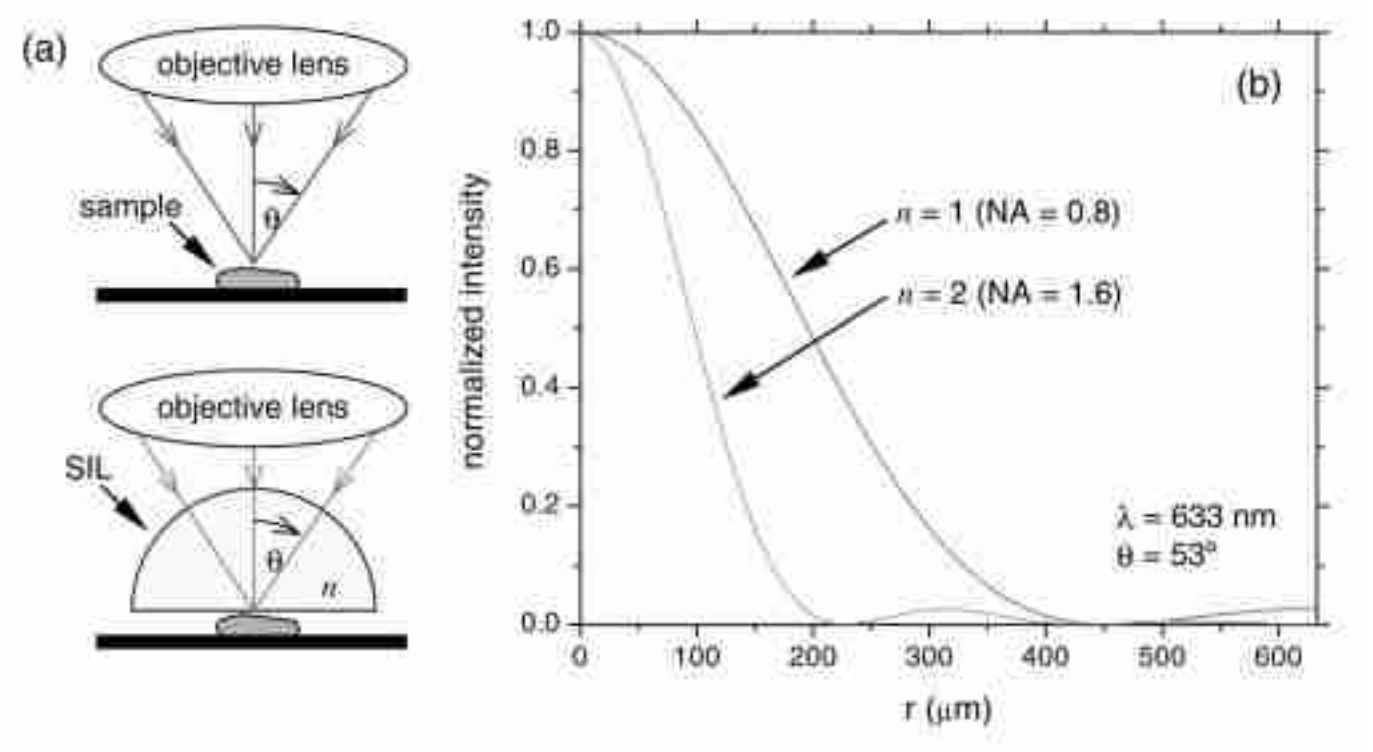

Fig. 1. Solid immersion microscopy. (a) Light is focused by an objective lens onto a sample in air with a maximum angle of incidence θ and through a hemispherical SIL with index of refraction n and the same angle θ. (b) The spot size in air with $\lambda = 633$ nm illumination $\theta = 53^\circ$ is decreased by a factor of 2 with a hemispherical solid immersion lens of $n = 2$.

Data storage applications of the SIL include magneto-optical and phase-change bit writing and reading. Mansfield *et al.* read bits from an optical disk with a $NA = 1.05$ hemispherical SIL [8], and Terris *et al.* used a superspherical SIL with $NA = 1.2$ to write 317-nm bits in a magneto-optic material [9]. Phase-change optical recording has been demonstrated by Hirota *et al.* using a hemispherical GaP SIL with $NA = 2.0$. Ghislain *et al.* exposed 190-nm lines in photoresist using a hemispherical SIL with a wavelength of $\lambda = 442$ nm [10].

B. Limitations of Large Solid Immersion Lenses

The spatial resolution of a conventional SIL is limited by lens aberrations and lens-sample separation. For optimum resolution, the surface to be imaged must be positioned within the near field of the SIL, where evanescent fields created by totally internally reflected rays decay exponentially. If topographical variations in the lens or sample cause separations greater than approximately 100 nm at visible wavelengths, the exponential decay and spreading of the focused fields in air reduce both transmittance and resolution. It is difficult to maintain uniform contact over a 30-μm-diameter field of view typical of a conventional SIL because of sample topography and nonplanarity of the lens surface adjacent to the sample. A solution to this problem, with improved optical transparency and increased tolerance to curvature and thickness errors, is scanning solid immersion microscopy with a microfabricated SIL.

Similar to scanning near-field optical microscopy and atomic force microscopy, scanning solid immersion microscopy with a SIL integrated onto a cantilever collects images serially by illuminating one point at a time [7]. A tip formed at the focus of the SIL localizes contact between the lens and sample while scanning, as shown in Fig. 2. For soft samples, the integrated SIL and cantilever can be held at a constant distance from the sample surface using force-feedback control. Microfabrication offers a method for batch fabrication of lenses with diameters on the order of microns. Silicon is an attractive lens material for scanning solid immersion microscopy because of its large index of refraction and well-developed micromachining technology base. The large refractive index enables us to obtain a large NA for high spatial resolution microscopy.

III. Microfabrication of a Silicon Solid Immersion Lens

Fabrication of a Si solid immersion lens with a cantilever and tip involves creating a smooth spherical microlens and patterning both sides of a thin Si cantilever. We develop a solvent reflow and reactive ion etch transfer method for fabricating microlenses on the order of 10 μm in diameter, and we use anodic bonding to a Pyrex wafer to access both sides of the cantilever.

A. Review of Microlens Fabrication Techniques

Arrays of microlenses have been fabricated for use in focal plane array CCD cameras, wavefront sensors, and fiber collimators [11], [12]. Photolithography is used to create refractive microlenses in both photosensitive polymers and substrates. Cylindrical pillars are defined in photoresist and heated to reflow the material into a curved shape. Popovic *et al.* used pedestals to control spreading of the lens during heating [13], and Daly *et al.* and Jay and Stern preformed the resist to define the lens shape prior to heating [14], [15]. To avoid contact angle limitations of

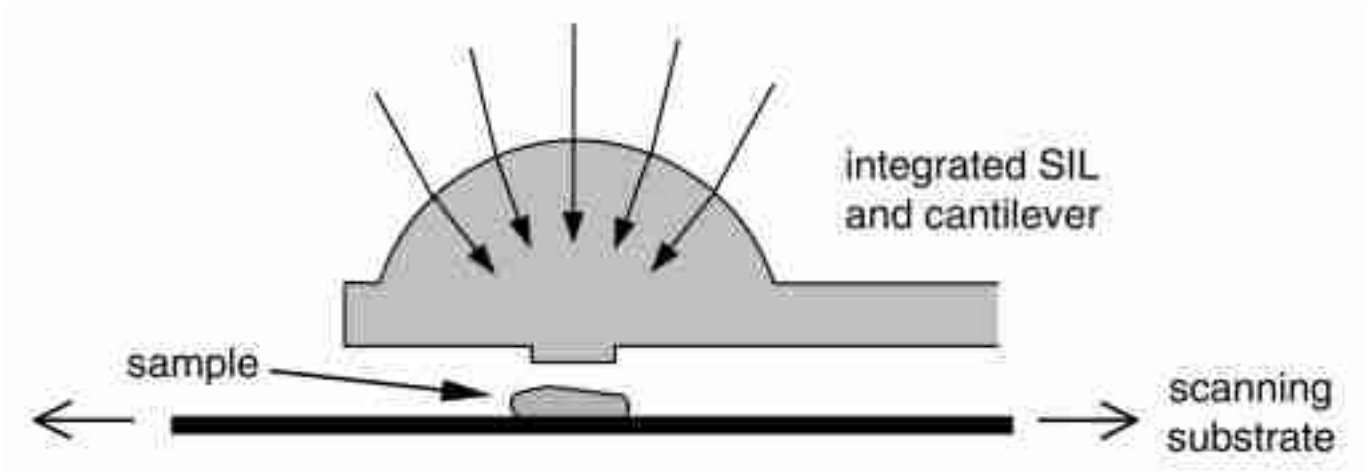

Fig. 2. Schematic of scanning solid immersion microscopy. Light is focused to a spot in the tip of an SIL mounted on a cantilever. A sample scanned close to the tip is imaged with the resolution of the focused spot.

thermal reflow methods, Erdmann and Efferenn used a photoresist solvent vapor to make 1 mm diameter lenses with 20 mm focal lengths [16]. The photoresist lens shape can be transferred into a substrate material with reactive ion etching (RIE). Savander demonstrated Si and glass lenses with NA less than 0.13 in air [17], and Jones *et al.* fabricated Si microlens arrays for use as concentrators in a CdHgTe infrared photodetector [18]. Techniques based on laser and electron beam writing have also been used to create refractive microlenses in a variety of materials [19]–[21]. Other refractive microlens fabrication techniques include lift-off, molding, the hydrophobic method, gradient index doping, and microjet printing [22]–[25].

B. Lens Formation

We fabricated the Si SIL and cantilever from the upper single-crystal Si layer of a silicon-on-insulator (SOI) wafer. The fabrication process flow is shown in Fig. 3. In Step 1, a photoresist pillar 5 μm in diameter is patterned in a mask aligner from 7-μm-thick photoresist. The pillar is reflowed by acetone vapor in a closed container at 20 °C for approximately 15 min. An initial quantity of 300 mL of liquid acetone per cubic meter of container volume is added. The acetone vaporizes and is absorbed by the photoresist, reducing its viscosity and causing it to reflow, as indicated in Step 2. The final shape of the pillar after reflow is a function of reflow time, acetone vapor concentration in the sealed container, and aspect ratio of the original photoresist pillar. Images of a photoresist pillar at three different times during the acetone reflow are shown in Fig. 4. After reflow, the photoresist is baked in a convection oven at 90 °C to drive out the solvents.

We etched lenses in the top single-crystal Si of the SOI wafer by transferring the photoresist lenses with RIE in Step 3. Transfer of a photoresist shape into Si requires control over the relative etch rates of resist and Si. Standard RIE recipes for Si are designed to be highly selective for Si with minimum removal of photoresist. Here an etch rate of photoresist comparable to that of Si is desired. A recipe based on CF_4 and O_2 gases was developed to enable control of the relative etch rates of silicon and photoresist. Equal etch rates for directly transferring the photoresist lens shape into Si are obtained with approximately equal flow rates of CF_4 and O_2 at a chamber pressure of 300 mT. The etch rates of Si and photoresist can be adjusted to create parabolic or aspheric lenses by altering the relative gas flow rates. In Step 4, a 0.3-μm-thick thermal oxide layer is grown on the lens above the glass transition temperature at 1100 °C to serve as an etch stop for the cantilever etch.

C. Tip and Cantilever Fabrication

A tip is needed opposite the lens at the focal point to localize the contact between lens and sample during scanning. To access the bottom side of the silicon lens, a Pyrex handle wafer is attached to the top Si of the SOI wafer. Trenches are first etched in the Pyrex wafer to protect the lenses during anodic bonding and to define the length of the cantilever. The Pyrex wafer is coated with a 1000-Å Cr sticking layer and patterned with photoresist, as indicated in Step 5. The Cr is removed from the Pyrex where the trenches are to be etched. Trenches approximately 10 μm deep are etched with a $HF/HNO_3/H_2O$ mixture. Step 5 finishes with stripping the photoresist and removing the remaining Cr. In Step 6, the Pyrex wafer with trenches is aligned over the lenses and anodically bonded at 900 V and 350 °C. The bulk Si of the SOI wafer is removed in Step 7 with a 14-h etch in 25% TMAH that stops on the buried oxide. The buried oxide is then cleared with 6:1 buffered oxide etch (BOE). Fig. 5 is an optical image of the Si lenses and thin film suspended over a trench in Pyrex.

A circular tip is patterned on the suspended Si membrane centered on the lens in Step 8. The size of the tip is varied by a procedure similar to that used for forming the lenses. The tips are etched in an isotropic CF_4/O_2 RIE in Step 9 leaving a flat top that compensates for possible misalignment of lens and tip during photolithography. In Step 10, 30-μm-wide cantilevers are patterned on the suspended Si film with the lens centered at the end. The cantilever is etched in an isotropic Cl_2CF_5 RIE in Step 11, stopping on the thermal oxide layer grown on the lens and cantilever in Step 4. The oxide is removed in 6:1 BOE to release the cantilevers. Individual die with integrated lenses and cantilevers are separated with a wafer saw in Step 12. A single lens and cantilever with a tip is shown in Fig. 6(a), and a one-dimensional array of integrated lenses and cantilevers is shown in Fig. 6(b).

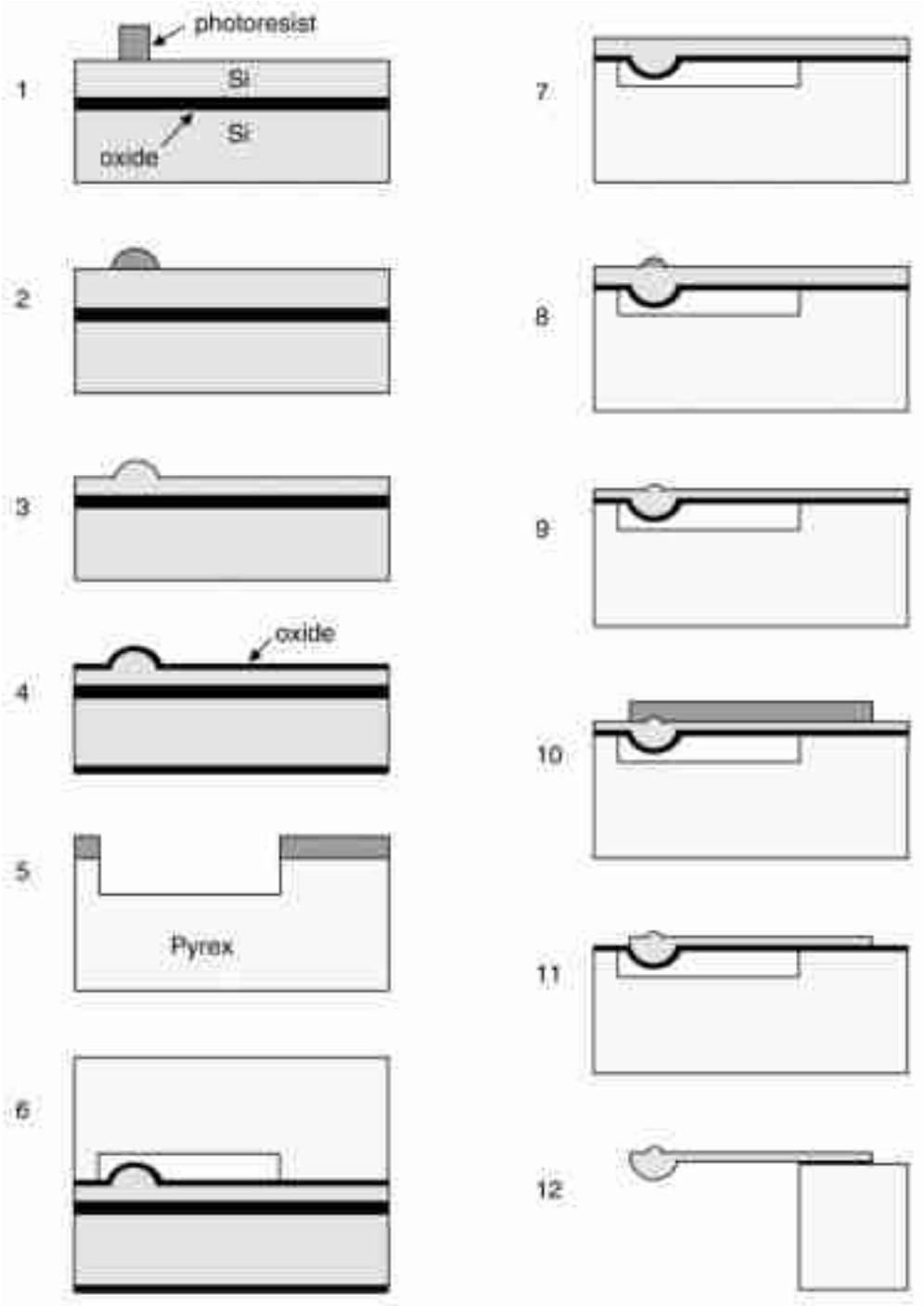

Fig. 3. Process flow for the microfabricated silicon solid immersion lens.

IV. Optical Performance of the SIL

Silicon solid immersion lenses 5–20 μm in diameter were fabricated according to the process described above. The integrated silicon cantilever is 30 μm wide, 3 μm thick, and extends beyond the Pyrex handle wafer approximately 150 μm. The tip fabricated below the lens is typically 1 μm tall with a flat top 2–4 μm in diameter. Though the spatial resolution of optical microscopy with the microfabricated Si SIL is governed by the size of the focused spot in Si rather than the tip diameter, a taller and sharper tip would be needed for scanning samples with tall, closely spaced features. The focus of the lens at the tip is approximately 3 μm below the geometrical center of the lens, which is with 20% of the ideal for a superspherical SIL. Several lenses were imaged with an AFM to characterize the shape and surface roughness of lenses made by the acetone reflow and RIE transfer technique. Root-mean-square (rms) variation in lens radius from the average of a best-fit sphere is less than 4%, as shown in Fig. 7. The rms surface roughness of the lens is estimated from the AFM scans to be less than 15 nm, which is better than $\lambda/40$ for $\lambda = 633$ nm.

A. Transmission

A solid immersion lens improves spatial resolution by focusing light through a high refractive-index material rather than

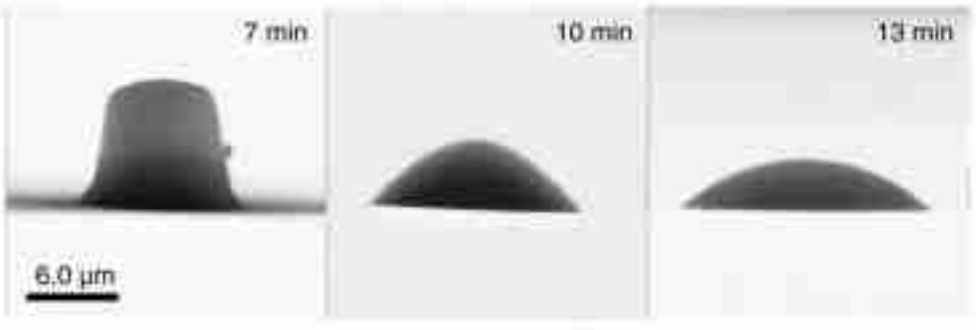

Fig. 4. Photoresist pillars reflowed in acetone vapor for three different lengths of time.

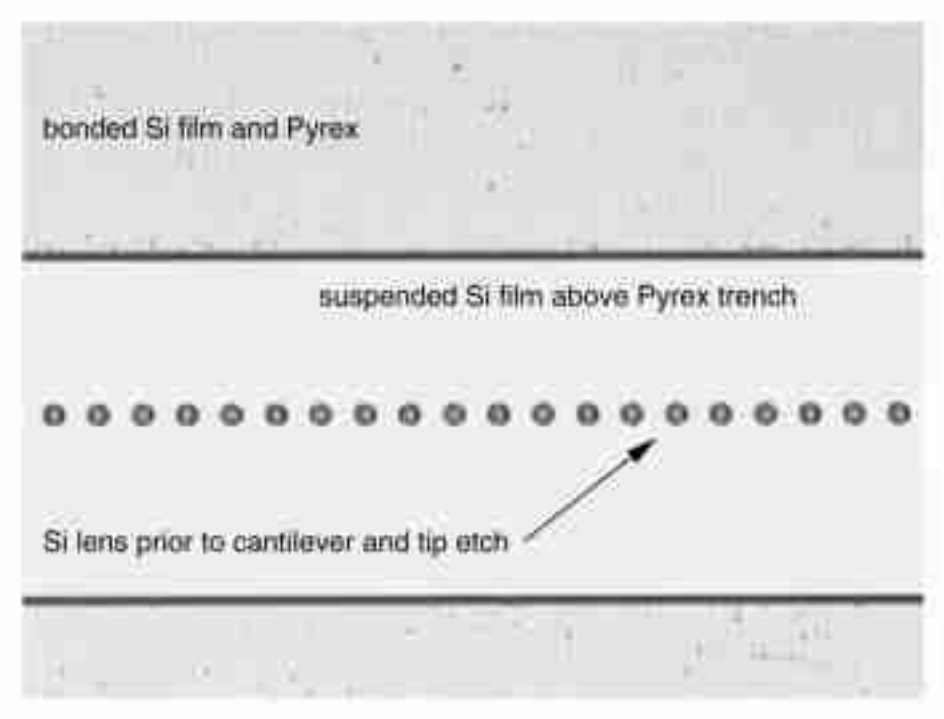

Fig. 5. Optical image of the top Si film with a one-dimensional array of Si lenses. The lenses are suspended over a trench in Pyrex after anodic bonding and removal of the bulk Si and middle oxide from the SOI wafer.

blocking light with a metal aperture. Losses in transmittance of a SIL are due to reflections and absorption. Silicon has an index of refraction $n = 3.4$ in the near- and mid-infrared spectrum, with absorption increasing for wavelengths less than $\lambda = 1000$ nm. If the thickness of an absorbing microlens is comparable to the penetration depth of the light, the lens can be used to focus wavelengths where the material is normally opaque. For a 5-μm-thick Si lens, less than 90% of the light is absorbed for wavelengths as small as nearly $\lambda = 600$ nm. We have demonstrated focusing and imaging with the SIL using a HeNe laser operating at $\lambda = 633$ nm. Though the penetration depth of Si is 2.7 μm at this wavelength, the 15-μm-diameter lens transmits approximately 3% of the incident light including surface reflections. This optical throughput is better than that of a tapered optical fiber with a metal aperture, where transmittance is typically worse than 10^{-4} [26]. The increase in absorption of Si with decrease in wavelength is accompanied by a rise in the real part of the refractive index. The real index of Si increases to $n = 3.9$ at $\lambda = 633$ nm from $n = 3.4$ at $\lambda = 1000$ nm. Use of the Si SIL for wavelengths greater than $\lambda = 1000$ nm eliminates absorption losses, leaving only reflection losses to reduce optical throughput.

B. Focusing

A lens cannot be used to focus light to a diffraction-limited spot in the presence of aberrations. However, the effect of aberrations is reduced in small lenses. Geometrically, a converging spherical wave will form a spot at the geometrical center of a spherical lens since all rays intersect the lens normal to its surface. Plane waves or off-axis converging waves incident on a spherical surface will experience spherical aberration where a ray striking the surface of the lens at a large angle to the surface normal focuses to a different point than a ray incident at a small angle to the surface normal. The spread of high- and low-angle rays focused to the optical axis broadens the lateral distribution of rays in the paraxial focal plane. This spread of rays prevents the lens from focusing to a diffraction-limited spot.

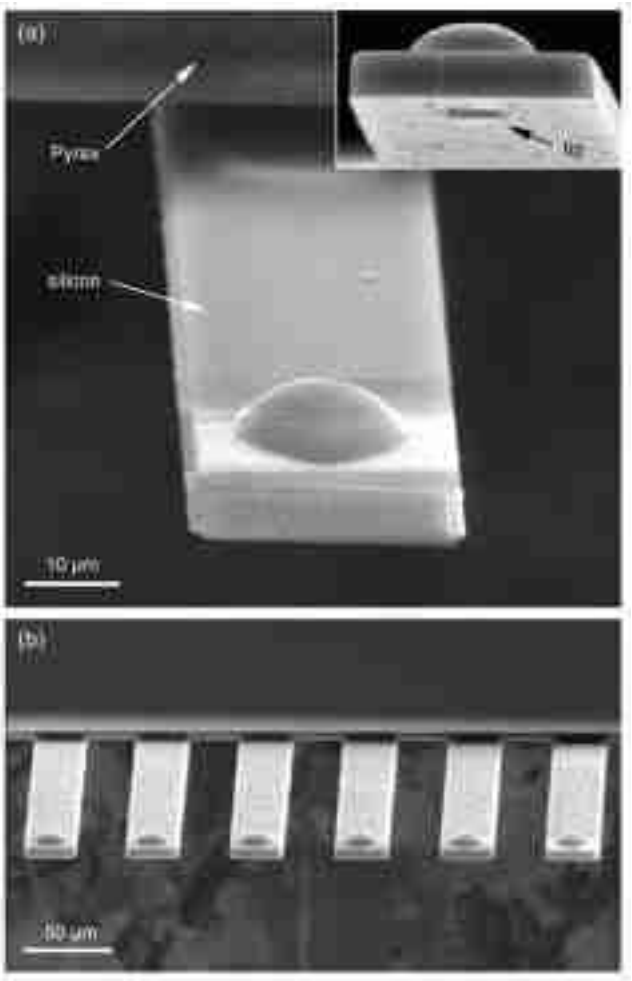

Fig. 6. SEM images of (a) the microfabricated Si solid immersion lens with a view of the tip inset and (b) a one-dimensional array of microfabricated Si solid immersion lenses.

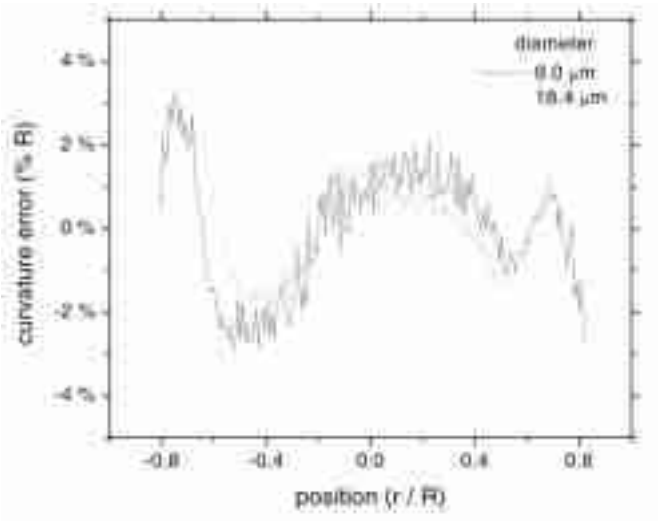

Fig. 7. Deviation in surface curvature of the SIL from spherical as a percentage of lens radius R. The surface topography of the lenses was obtained with an AFM.

Consider a ray in air parallel to the Z-axis incident on a sphere of diameter d and index n, as shown in Fig. 8. A radius through the point of intersection on the lens surface makes an angle β with an axis parallel to the ray. This ray is refracted at the lens surface and focused at a point z behind the geometrical center of the sphere, making an angle θ with the axis. Paraxial rays form a spot at the paraxial focus at z_p given by

$$z_p = \frac{d}{2}\left(\frac{1}{n-1}\right). \tag{1}$$

The focal spread along the optical axis can be obtained from the difference between the focal positions of a ray at an angle β to the surface and a paraxial ray in the sphere according to [27]

$$z_p - z = \frac{d}{2}\left[\frac{1}{n-1} - \frac{\sin(\beta-\theta)}{\sin(\theta)}\right]. \tag{2}$$

Note that the focal spread along the optical axis is directly proportional to sphere diameter d. Lateral focal spread y at the paraxial focus can be obtained from $y = (z_p - z)\tan\theta$ and is also directly proportional to the sphere diameter.

The lateral spread of rays at the paraxial focus can be decreased by reducing the sphere diameter or by increasing the lens refractive index. Spherical aberrations no longer limit the spot size when the focal spread y becomes comparable to half the diffraction-limited spot size $s = \lambda/(2NA)$. The diameter at which this occurs can be estimated to be

$$d \approx \frac{\lambda(n-1)}{2n}\left[\frac{\cot\theta}{\sin\theta - (n-1)\sin(\beta-\theta)}\right] \tag{3}$$

where θ is the maximum angle of incidence. When $\sin\theta = 0.8$ $(\theta = 53.1^\circ)$ and the lens refractive index is $n = 3.4$, the lateral spread due to spherical aberration is comparable to the diffraction limited spot size when $d \approx 4\lambda$. We have investigated the reduction in spherical aberration of small lenses more rigorously with Mie theory and found similar results [27].

We demonstrated focusing of a nearly plane wave with a 15-μm-diameter microfabricated Si SIL at $\lambda = 633$ nm. As diagrammed in Fig. 9(a), a HeNe laser is focused to a spot with an illumination lens $(NA = 0.03)$, and the spot is imaged with a collection objective $(NA = 0.8)$ and CCD camera. The Si SIL is inserted at the focus, and its effect on the beam is recorded with the CCD. The low NA lens that illuminated the SIL creates a nearly planar incident wave at the surface of the lens. Assuming a paraxial Gaussian beam, the radius of curvature of the incident wave is estimated to be greater than 17 mm [28], which is more than 3 orders of magnitude larger than the lens radius of curvature. Fig. 9(c) shows the focused spot with and without the lens. Normalized profiles of the spots fit to Gaussian curves are shown in Fig. 9(b). While a 1-mm-diameter spherical lens is expected to have a 30-μm focal spread at the paraxial focus due to spherical aberration, the FWHM of the spot with the Si SIL is close to one wavelength. The SIL reduces the spot FWHM by a factor of 15.7.

C. Imaging

To achieve spatial resolution below the diffraction limit in air, the Si SIL must be held within the near field of the sample. Visible imaging with a 15-μm-diameter microfabricated Si SIL was demonstrated at $\lambda = 633$ nm by scanning a grating below the

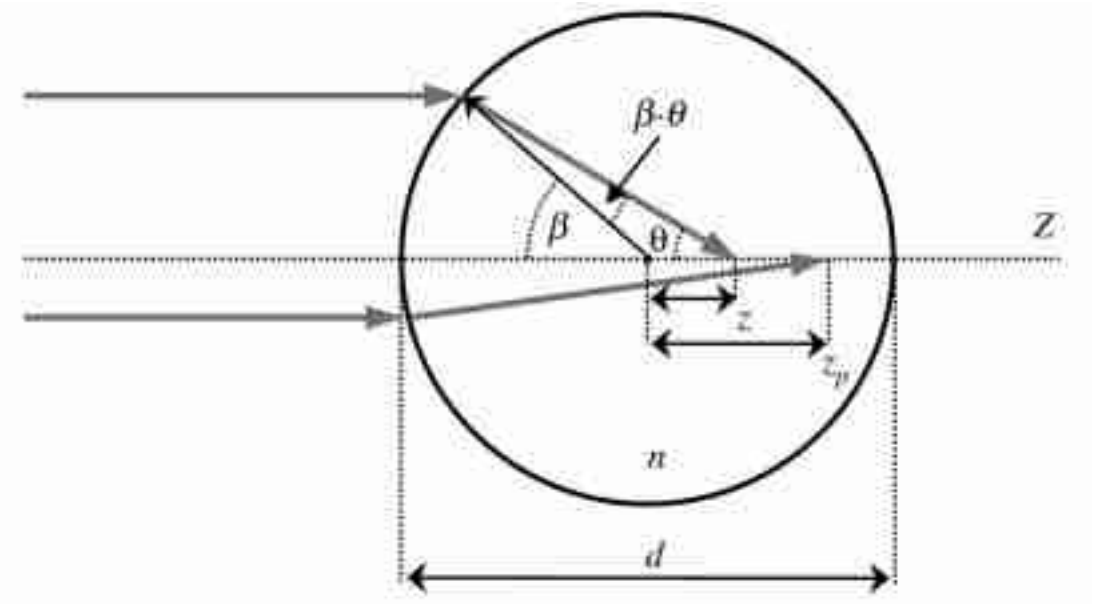

Fig. 8. Parallel rays incident on a spherical lens of diameter d and refractive index n showing spherical aberration. Rays are refracted at an angle θ to the optical axis and focused to a point z from the geometrical center. Rays incident at a small angle β converge at the paraxial focus a distance z_p from the geometrical center.

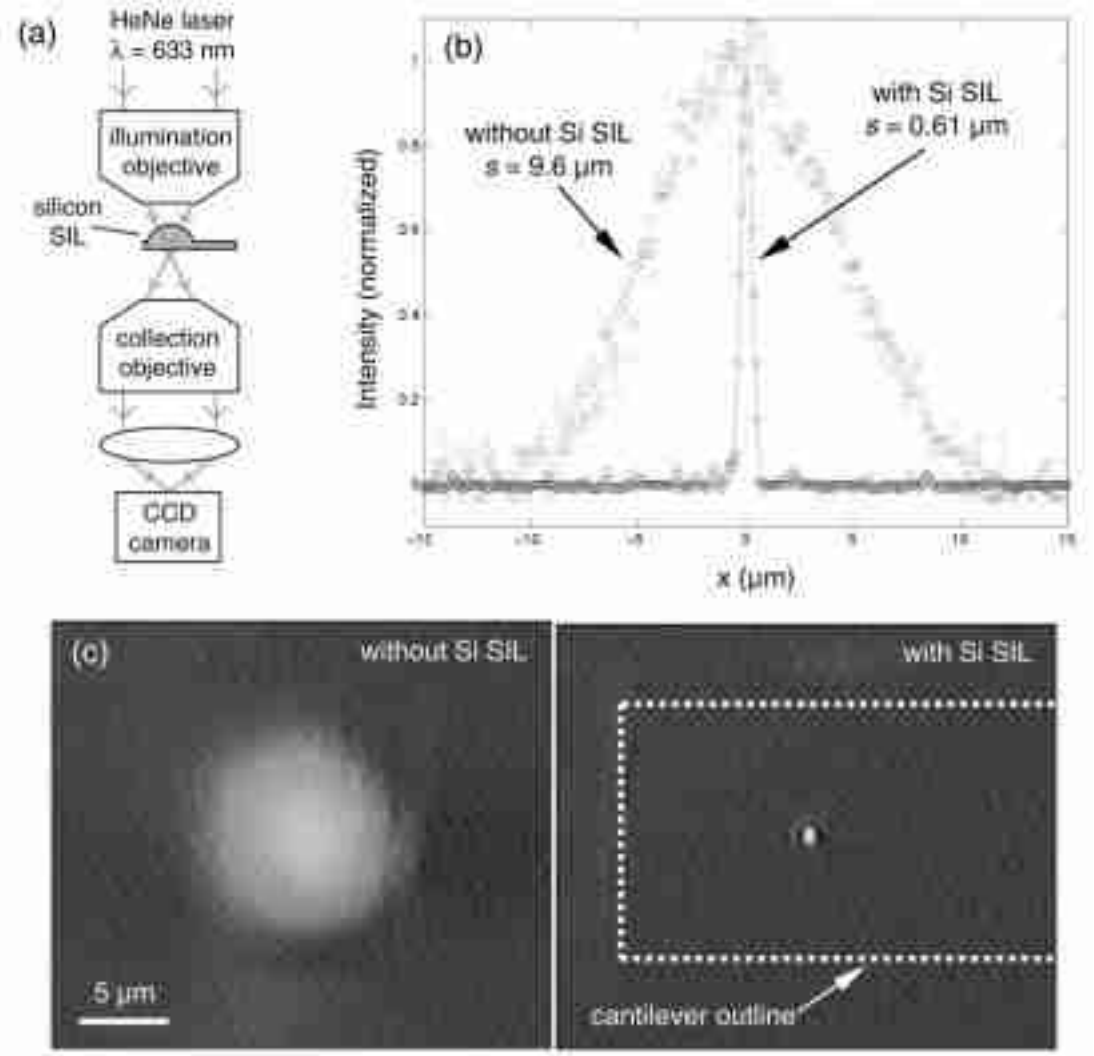

Fig. 9. focusing with the microfabricated Si solid immersion lens at a wavelength of $\lambda = 633$ nm. (a) Experimental apparatus in which light from a HeNe laser is focused with a $NA = 0.03$ illumination objective onto the Si SIL and imaged with a $NA = 0.8$ collection objective and CCD camera. (b) Intensity profiles of the HeNe beam with and without the Si SIL fit to a Gaussian curve showing a spot close to the wavelength in diameter. (c) Optical images of the HeNe beam with and without the Si SIL.

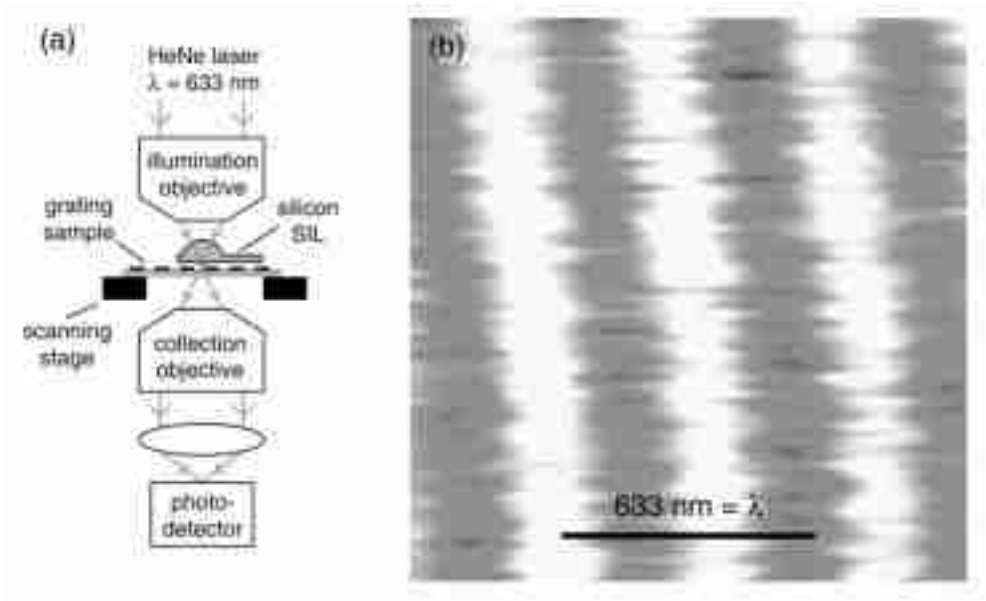

Fig. 10. Near-field imaging with the microfabricated Si solid immersion lens at a wavelength of $\lambda = 633$ nm. (a) Experimental apparatus in which light from a HeNe laser is focused with a $NA = 0.8$ illumination objective through the Si SIL onto the grating and imaged with a $NA = 0.8$ collection objective and photodetector. (b) Two-dimensional image of a 200-nm linewidth grating taken in transmission with the scanned Si SIL showing resolution below the diffraction limit in air.

tip of the SIL and collecting transmitted light. The grating is 1000-Å-thick Ti lines on quartz with a linewidth of 200 nm. It is scanned in contact with the SIL in the microscope diagrammed in Fig. 10(a). A HeNe laser is focused by an illumination objective $(NA = 0.8)$ into the SIL above the grating, and light passing through the grating is gathered by a collection objective $(NA = 0.4)$ and measured with a photodetector. A chopper and lock-in amplifier are used to improve the signal-to-noise ratio (SNR).

Fig. 10(b) shows a two-dimensional scan of the 200-nm linewidth grating resolved by the microfabricated Si SIL. The normalized transmitted intensity ranged from 0.35 over a line to 0.65 over a space, where 0.5 is the average transmittance. We found the spatial resolution of the image taken with the SIL to be a factor of 2.8 greater than the same image taken without the SIL. Improvement in resolution by a maximum of 3.9 may be possible with a larger maximum illumination angle and perfect alignment. The Si SIL can also be operated in the infrared where Si is transparent. We have demonstrated infrared imaging with a spot size of $\lambda/5$ at $\lambda = 9.3$ μm [29] and refraction contrast imaging at $\lambda = 10.7$ μm with spatial resolution of $\lambda/4$ [30].

V. Conclusion

We present the microfabrication of a solid immersion lens from silicon for scanning near-field optical microscopy. The lens is shaped from photoresist reflowed in acetone vapor and transferred into single-crystal Si by reactive ion etching. We show that the microfabricated Si SIL can focus visible light at $\lambda = 633$ nm when its thickness is comparable to the penetration depth of the light and that the SIL can focus a plane wave to a spot close to the wavelength in diameter. We demonstrate scanning near-field optical microscopy with the Si SIL by imaging 200-nm lines with $\lambda = 633$ nm light. Applications of scanning solid immersion microscopy with a microfabricated Si SIL include microscopy, thermometry, and spectroscopy.

References

[1] E. Betzig and J. K. Trautman, "Near-field optics: microscopy, spectroscopy, and surface modification beyond the diffraction limit," *Science*, vol. 257, p. 189, 1992.

[2] S. M. Mansfield and G. S. Kino, "Solid immersion microscope," *Appl. Phys. Lett.*, vol. 57, pp. 2615–2616, 1990.

[3] T. R. Corle and G. S. Kino, *Confocal Scanning Optical Microscopy and Related Imaging Systems*. San Diego, CA: Academic, 1996.

[4] B. Richards and E. Wolf, "Electromagnetic diffraction in optical systems II: Structure of the image field in an aplanatic system," in *Proc. Royal Soc. A*, vol. 253, 1959.

[5] T. Sasaki, M. Baba, M. Yoshita, and H. Akiyama, "Application of solid immersion lens to high-resolution photoluminescence imaging of patterned GaAs quantum wells," *Jpn. J. Appl. Phys. Part 2-Lett.*, vol. 36, pp. L962–L964, 1997.

[6] Q. Wu, G. D. Feke, R. D. Grober, and L. P. Ghislain, "Realization of numerical aperture 2.0 using a gallium phosphide solid immersion lens," *Appl. Phys. Lett.*, vol. 75, pp. 4064–4066, 1999.

[7] L. P. Ghislain and V. B. Elings, "Near-field scanning solid immersion microscope," *Appl. Phys. Lett.*, vol. 72, pp. 2779–2781, 1998.

[8] S. M. Mansfield, W. R. Studenmund, G. S. Kino, and K. Osato, "High numerical aperture lens system for optical storage," *Opt. Lett.*, vol. 18, pp. 305–307, 1993.

[9] B. D. Terris, H. J. Mamin, D. Rugar, W. R. Studenmund, and G. S. Kino, "Near-field optical data storage using a solid immersion lens," *Appl. Phys. Lett.*, vol. 65, pp. 388–390, 1994.

[10] L. P. Ghislain, V. B. Elings, K. B. Crozier, S. R. Manalis, S. C. Minne, K. Wilder, G. S. Kino, and C. F. Quate, "Near-field photolithography with a solid immersion lens," *Appl. Phys. Lett.*, vol. 74, pp. 501–503, 1999.

[11] Y. Sano, T. Nomura, H. Aoki, and S. Terakawa, "Submicron spaced lens array process technology for a high photosensitivity CCD image sensor," *Optoelectron. Devices Technol.*, vol. 6, pp. 219–229, 1991.

[12] M. E. Motamedi, "Micro-opto-electro-mechanical systems," *Optic. Eng.*, vol. 33, pp. 3505–3517, 1994.

[13] Z. D. Popovic, R. A. Sprague, and G. A. N. Connell, "Technique for monolithic fabrication of microlens arrays," *Appl. Opt.*, vol. 27, pp. 1281–1284, 1988.

[14] D. Daly, R. F. Stevens, M. C. Hutley, and N. Davies, "The manufacture of microlenses by melting photoresist," *Measure. Sci. Technol.*, vol. 1, pp. 759–766, 1990.

[15] T. R. Jay and M. B. Stern, "Preshaping photoresist for refractive microlens fabrication," *Optic. Eng.*, vol. 33, pp. 3552–3555, 1994.
[16] L. Erdmann and D. Efferenn, "Technique for monolithic fabrication of silicon microlenses with selectable rim angles," *Optic. Eng.*, vol. 36, pp. 1094–1098, 1997.
[17] P. Savander, "Microlens arrays etched into glass and silicon," *Opt. Lasers Eng.*, vol. 20, pp. 97–107, 1994.
[18] C. L. Jones, B. E. Matthews, D. R. Purdy, and N. E. Metcalfe, "Fabrication and assessment of optically immersed CdHgTe detector arrays," *Semiconduct. Sci. Technol.*, vol. 6, pp. C110–C113, 1991.
[19] V. Lyubin *et al.*, "Novel effects in inorganic As50Se50 photoresists and their application in micro-optics," *J. Vacuum Sci. Technol. B*, vol. 15, pp. 823–827, 1997.
[20] S. Babin, M. Weber, and H. W. P. Koops, "Fabrication of a refractive microlens integrated onto a monomode fiber," *J. Vacuum Sci. Technol. B*, vol. 14, pp. 4076–4079, 1996.
[21] A. Y. Smuk and N. M. Lawandy, "Direct laser fabrication of dense microlens arrays in semiconductor-doped glass," *J. Appl. Phys.*, vol. 87, pp. 4026–4030, 2000.
[22] T. Serikawa and S. Shirai, "Modeling of lift-off sputter deposition and application to fabrication of a microlens," *Thin Solid Films*, vol. 281–282, pp. 246–248, 1996.
[23] D. M. Hartmann, O. Kibar, and S. C. Esener, "Characterization of a polymer microlens fabricated by use of the hydrophobic effect," *Opt. Lett.*, vol. 25, pp. 975–977, 2000.
[24] T. Katayama, Y. Munetaka, and K. Iga, "Improvement of electric-field-assisted ion exchange method for planar microlens array fabrication," *Jpn. J. Appl. Phys. Part 1-Regular Papers Short Notes Rev. Papers*, vol. 38, pp. 775–776, 1999.
[25] Y. Ishii, S. Koike, Y. Arai, and Y. Ando, "Ink-jet fabrication of polymer microlens for optical-I/O chip packaging," *Jpn. J. Appl. Phys. Part 1-Regular Papers Short Notes Rev. Papers*, vol. 39, pp. 1490–1493, 2000.
[26] L. Novotny, D. W. Pohl, and B. Hecht, "Scanning near-field optical probe with ultra-small spot size," *Opt. Lett.*, vol. 20, pp. 970–972, 1995.
[27] D. A. Fletcher, K. E. Goodson, and G. S. Kino, "Focusing in microlenses close to a wavelength in diameter," Opt. Lett., vol. 26, pp. 399–401, 2001.
[28] A. E. Siegman, *Lasers*. Sausalito: University Science Books, 1986.
[29] D. A. Fletcher, K. B. Crozier, G. S. Kino, C. F. Quate, K. E. Goodson, D. Simanovskii, and D. V. Palanker, "Near-field infrared imaging with a microfabricated solid immersion lens," *Appl. Phys. Lett.*, vol. 77, pp. 2109–2111, 2000.
[30] D. A. Fletcher, K. B. Crozier, C. F. Quate, G. S. Kino, K. E. Goodson, D. Simanovskii, and D. V. Palanker, "Refraction contrast imaging with a scanning microlens," *Appl. Phys. Lett.*, vol. 78, pp. 3589–3591, 2001.

Daniel A. Fletcher received the B.S.E. degree in mechanical and aerospace engineering *(summa cum laude)* from Princeton University, Princeton, NJ, in 1994 and the D.Phil. degree in engineering science from the University of Oxford, Oxford, U.K., in 1997. He received the Ph.D. degree in mechanical engineering from Stanford University, Stanford, CA, in 2001.

He is currently a Research Associate at Stanford University.

Kenneth B. Crozier received the B.Sc. degree and B.E. (Honors) degree in physics and electrical engineering, respectively, from the University of Melbourne, Australia, in 1996 and the M.S.E.E. degree in electrical engineering from Stanford University, Stanford, CA, in 1999. He is currently pursuing the Ph.D. degree in electrical engineering at Stanford University in the research group of Professor C. F. Quate.

In 1997, he was employed by the Department of Electrical Engineering at the University of Western Australia. His research interests include micromachining and scanning probe microscopy.

Kathryn W. Guarini (M'00) received the B.S. degree in applied physics from Yale University, New Haven, CT, in 1994 and the Ph.D. degree in applied physics from Stanford University, Stanford, CA, in 1999.

She is a Research Staff Member in the Silicon Technology Department at IBM Research, Yorktown Heights, NY. Her research interests include novel transistor devices and fabrication techniques, nanoscience and nanotechnology, self-assembly, and high-resolution lithography.

Stephen C. Minne received the B.S. degree with highest honors from the University of Illinois, Urbana-Champaign, in 1992 and the M.S. and Ph.D. degrees from Stanford University, Stanford, CA, in 1994 and 1996, respectively.

His current research focuses on increasing the throughput of the atomic force microscope (AFM). By fabricating massively parallel arrays of highly functional AFM cantilevers, he and his co-workers have been able to increase the tip speed of the AFM by a factor of 100, and the imaged area by a factor of 100. He currently is President and Co-Founder of NanoDevices, Inc., and holds a position as a Consulting Professor at Stanford University. He has published over 20 papers and coauthored a book on improving the speed of the AFM, has 11 patents pending or issued in the field of AFM, and has given numerous domestic and international talks on the subject.

Dr. Minne has received the Leland T. Edwards Fellowship from 1992 to 1996, and has membership in many professional and academic societies.

Gordon S. Kino (S'52–A'54–SM'63–F'66–LF'94) received the B.Sc. and M.Sc. degrees in mathematics from London University, U.K., and the Ph.D. degree in electrical engineering from Stanford University, Stanford, CA.

He is the W. M. Keck Foundation Professor of Electrical Engineering, Emeritus, and Professor, by Courtesy, of Applied Physics, Emeritus. He was the Director of the E. L. Ginzton Laboratory at Stanford University. He has worked on microwave tubes, electron guns, plasmas, the Gunn effect, acoustic devices, acoustic imaging, nondestructive testing, fiber-optics, and microscopy; his current interests are in various forms of microscopy, acoustic devices, fiber optics, and optical storage. He has published over 430 papers and 47 patents. He and his students have developed new types of scanning optical microscopes and interferometric microscopes. He and T. Corle are the authors of *Confocal Optical Microscopy and Related Techniques* (New York: Academic, 1996), and he is the author of *Acoustic Waves: Devices, Imaging, and Analog Signal Processing* (Englewood Cliffs, NJ: Prentice-Hall, 1987).

Dr. Kino was a Guggenheim Fellow in 1967. He is a Fellow of the American Physical Society and the AAAS, and a member of the National Academy of Engineering. In 1984, he received the IEEE Sonics and Ultrasonics Group Achievement Award and in 1986, he received the ASNT Achievement Award in Applied Research.

Calvin F. Quate (S'43–A'50–M'55–F'65–LF'89) received the B.S. degree from the University of Utah, Salt Lake City, and the Ph.D. degree from Stanford University, Stanford, CA.

He is the Leland T. Edwards Professor of Electrical Engineering at Stanford University, Stanford, CA. His research centers on the development and application of scanning probe microscopes.

Kenneth E. Goodson (M'95–A'96) received Bachelor's degrees in mechanical engineering and humanities from the Massachusetts Institute of Technology (MIT), Cambridge, along with the Sudler Prize in 1989. He received the M.S. and Ph.D. degrees in mechanical engineering from MIT in 1991 and 1993, respectively, with a dissertation on self-heating of silicon-on-insulator transistors.

He is an Associate Professor of Mechanical Engineering at Stanford University, Stanford, CA. Before joining Stanford University in 1994, he worked with the Materials Research Group at Daimler-Benz AG on the thermal design of power circuits for vehicles. His Stanford University's research group, which includes 15 students and postdoctoral scholars, studies heat transfer in electronic systems with a focus on microscale conduction in novel thin films, transistors, and interconnect systems. In addition, he leads a multi-investigator DARPA/Intel/Stanford University effort on two-phase microchannel cooling for computers. He is coauthor of 80 archival journal articles and conference papers and four book chapters. In spring 1996, he was a JSPS Visiting Professor at the Tokyo Institute of Technology.

Dr. Goodson is a recipient of the ONR Young Investigator Award in 1996, the NSF CAREER Award in 1996, and the Outstanding Reviewer Award from the ASME Journal of Heat Transfer in 1999.